

Thermal hologram fixing in pure and doped KNbO₃ crystals

G. Montemezzani and P. Günter

Institute of Quantum Electronics, Swiss Federal Institute of Technology, ETH Hönggerberg, CH-8093 Zürich, Switzerland

Received May 15, 1990; accepted July 9, 1990

We demonstrate holographic fixing by means of a thermal cycling procedure in pure and doped photorefractive KNbO₃ crystals. At elevated temperatures (70–100°C) the photoinduced grating is compensated for by a secondary grating that is formed by charge carriers whose thermal activation energy is ~1.0 eV. The secondary carriers are stable at room temperature and form the fixed grating after cooling the crystal. They are believed to be represented by ions or ion vacancies. By using our fixing mechanisms the holographic storage time in KNbO₃ can be increased by a factor of 10⁶.

1. INTRODUCTION

It was demonstrated several years ago that KNbO₃ is one of the best materials for dynamic holography^{1,2} because of its combination of large electro-optic coefficients³ and high photoconductivity.⁴ High photosensitivity⁵ and photoconductive-drift lengths that are comparable with fringe spacings⁶ in holographic experiments were found in this material. Difficulties in the commercial availability of high-quality samples prevented the use of KNbO₃ for holographic applications. Since KNbO₃ crystals can now be obtained from several companies, there is a renewed interest in this material for such applications. The best photorefractive properties are normally achieved in Fe-doped crystals reduced by an electrochemical method.⁴ The large photoconductivity of KNbO₃ is responsible for the observed fast recording times and for the relatively fast erasure times of the hologram during readout. However, for various applications, e.g., in the fields of optical signal processing and associative memories, a nondestructive readout of the stored information is needed. The purpose of this study is to demonstrate the feasibility of using KNbO₃ as a crystal for long-term storage also.

Several techniques for fixing holographic gratings in electro-optic crystals were developed in the past, such as thermal fixing in LiNbO₃ (Refs. 7 and 8) and Bi₁₂SiO₂₀ (BSO),⁹ electrical fixing in BaTiO₃ (Ref. 10) and strontium barium niobate (SBN),^{11,12} two-photon recording in LiNbO₃ (Ref. 13) and potassium tantalate niobate (KTN),¹⁴ as well as thermal fixing combined with the application of an ac electric field in Bi₁₂TiO₂₀ (BTO).¹⁵ Additionally, quasi-nondestructive readout of the stored information can be obtained by a fixing technique in BSO and BTO crystals at room temperatures.^{16–19}

In a recent paper²⁰ we reported an anomalous behavior during the recording and the subsequent dark decay of holographic gratings in pure KNbO₃ at temperatures near 100°C. The anomalous dynamics of the holographic diffraction efficiency could not be explained by the classical models for the photorefractive effect, where a single set of donor and acceptor centers is assumed. It could only be

understood through the presence of some charge carriers that can move at elevated temperatures, creating a negative replica of the photoinduced space-charge field. At room temperature these carriers have an extremely low drift velocity, which permits the fixing of the holographic grating.

In this paper we report on new experiments that extend the previous work to doped KNbO₃ crystals. We focus on the optimization of the fixing properties and on the determination of the activation energies for the compensating charge carriers in the different crystals. Comparing the different results and assuming a common origin for fixing in all the investigated samples, we can limit the range of the possible origins for the secondary charge carriers.

2. EXPERIMENTS

The three crystals used in our experiments were grown in our laboratories by the method of top-seeded high-temperature-solution growth.²¹ One of the three crystals investigated was nominally pure; the second was doped with a 1% Fe concentration in the melt (KNbO₃:Fe). The melt composition of the third crystal was $K_{0.95}Li_{0.025}Na_{0.025}NbO_3 + 1000$ parts in 10^6 Fe (KNbO₃:LiNaFe). In the third crystal, Fe was added in order to maintain good photorefractive properties. From the as-grown boules, rectangular shaped crystals were cut, and their faces parallel to the *c* axis were polished to optical quality. The thicknesses of the pure, the KNbO₃:Fe, and the KNbO₃:LiNaFe samples were 1.43, 2.12, and 1.54 mm, respectively.

Measurements of optical absorption, dark conductivity and photoconductivity, beam coupling, and isotropic Bragg diffraction at room and elevated temperature were performed. The setup for the holographic experiments is shown in Fig. 1. The angle between the two expanded Ar⁺ beams ($\lambda = 514.5$ nm) in all experiments was $\theta = 8.4^\circ$, giving a grating spacing of $\Lambda = 1.75$ μ m. The grating vector was oriented along the *c* axis of the crystals. The hologram was read out with a weak He–Ne laser

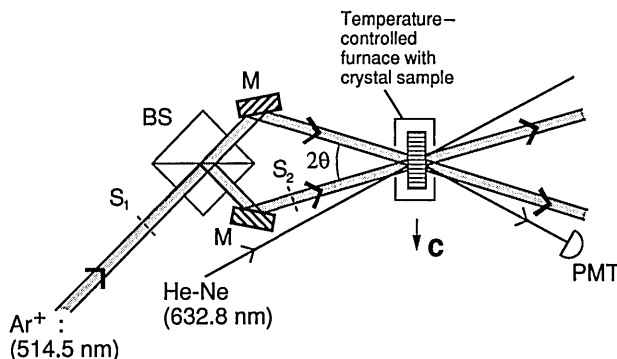


Fig. 1. Setup used for the holographic experiments. BS, beam splitter; M, mirrors; S₁, S₂, shutters; PMT, photomultiplier.

beam ($\lambda = 632.8$ nm) incident under the Bragg angle. The dark decay (with shutter S₁ of Fig. 1 closed) was also monitored by the He-Ne beam. The diffraction efficiency η , defined as the ratio of the diffracted-wave intensity to the incident-wave intensity, was measured by a photomultiplier tube. The data were then digitized by using either a digital oscilloscope or a digital multimeter and were transferred to a computer. For the beam-coupling measurements the intensity I_A of one of the recording beams was attenuated by inserting a neutral-density filter in front of the crystal. The transmitted intensity [$I_A(L)$, where L is the crystal thickness] was detected by an additional photomultiplier behind the crystal. In this way the effective gain γ_0 , defined as

$$\gamma_0 = \frac{I_A(L)^{\text{with pump}}}{I_A(L)^{\text{without pump}}} \equiv \exp(\Gamma L), \quad (1)$$

was measured. Γ is the exponential gain coefficient arising from beam coupling.

In the Bragg-diffraction experiments the polarization of the recording beams was perpendicular to the plane of incidence and that of the weak readout beam was parallel to the plane of incidence. For the beam-coupling experiments the writing beams also were polarized parallel to the incidence plane in order to make use of the large electro-optic coefficient r_{33} .

To characterize the unusual dynamical behavior, we performed various measurements at temperatures ranging between 20° and 180°C. For this purpose the samples were placed in a furnace that permitted a temperature stability of 0.05°C. No electric field was applied to the samples, so the main mechanisms for the charge transport were thermal diffusion of the carriers, drift due to internal electric fields produced by the periodic illumination, and the photovoltaic effect.

3. RESULTS

The measured absorption constants α at 514 nm for the undoped, the Fe-doped, and the LiNa- and Fe-doped KNbO₃ samples were 0.25, 1.0, and 0.5 cm⁻¹, respectively. No qualitative difference in the absorption spectra of the two doped samples was observed, which suggests a common origin for the photorefractive active centers. As is usual for KNbO₃ crystals,²² the doped samples exhibited a smaller dark conductivity σ_d as well as a smaller mobility-lifetime product than the pure, partially reduced sample.

We measured $\sigma_d = 4 \times 10^{-10}$ (Ω cm)⁻¹ for the pure sample, $\sigma_d = 2 \times 10^{-13}$ (Ω cm)⁻¹ for KNbO₃:Fe, and $\sigma_d = 3 \times 10^{-13}$ (Ω cm)⁻¹ for KNbO₃:LiNaFe. The value of $\Phi\mu\tau$ (where Φ is the quantum efficiency, μ is the mobility, and τ is the lifetime of the excited carriers) obtained from photoconductivity measurements⁴ was 6×10^{-9} cm²/V for the pure sample and 300 times smaller for a doped sample.

Both electrons and holes can contribute to the photoconductivity in KNbO₃.⁴ In general, the photoconductivity σ_{ph} is given by²³

$$\sigma_{ph} = n_e e \mu_e + n_h e \mu_h = g_e \tau_e e \mu_e + g_h \tau_h e \mu_h, \quad (2)$$

where e is the elementary charge, n_e and n_h are the densities of photoexcited carriers, μ_e and μ_h are the mobilities, g_e and g_h are the generation rates, and τ_e and τ_h are the lifetimes for electrons and holes, respectively. The relative contributions of the first and second terms on the right-hand side of Eq. (2) depend strongly on the doping and on the reduction states of the crystals. In general,^{4,22} the first term dominates in strongly reduced KNbO₃ crystals and the second in strongly doped, as-grown samples. With consideration of the geometry used, the sign of the charge carriers responsible for the photoinduced space-charge field (primary charge carriers) can be deduced from beam-coupling experiments.²⁴ In our samples we found charge transport that is due to holes in both doped crystals and electron charge transport in the pure crystal.

At room temperature the buildup, the dark decay, and the optical erasure of the space-charge field ($E_{sc} \propto \eta^{1/2}$) follow the normal simple exponential time behavior illustrated in Fig. 2. The recording process is given by $E_{sc}(t) = C[1 - \exp(-t/\tau_{\text{writing}})]$. The decay and erasure are given by $E_{sc}(t) = C \exp(-t/\tau_2)$, where τ_2 is the respective time constant. The same dynamics is expected to appear also if the recording is carried out at elevated temperatures. However, at temperatures above 70°C the single-exponential buildup and decay seen in Fig. 2 are reproduced only if the hologram recording is interrupted immediately after E_{sc} has reached its saturation value. If the recording is prolonged, the steady-state refractive-index change is no longer stable and the diffraction efficiency begins to decrease. This is observed in all three samples at elevated temperatures and in the KNbO₃:Fe sample even at room temperature. The typical behavior

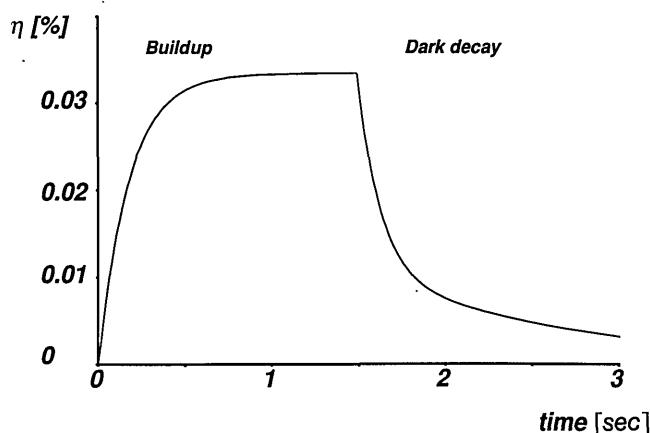


Fig. 2. Holographic recording and dark erasure cycle of pure KNbO₃ at room temperature. Recording intensity 25 mW/cm².

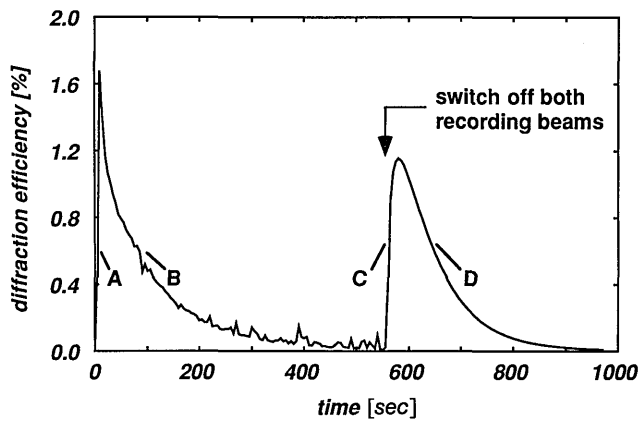


Fig. 3. Time dependence of the diffraction efficiency during recording ($t < 550$ sec) and decay in the dark ($t > 550$ sec) in $\text{KNbO}_3:\text{LiNaFe}$ at $T = 95^\circ\text{C}$. A, The photoinduced space-charge field is generated. B, Secondary charge carriers compensate the primary grating. C, The photoinduced field disappears. D, The secondary grating decays thermally. The same dynamics is observed in pure KNbO_3 and in Fe-doped KNbO_3 as well.

for the recording ($t < 550$ sec) and the subsequent development of the diffraction efficiency in the dark ($t > 550$ sec) can be seen in Fig. 3 for the case of the $\text{KNbO}_3:\text{LiNaFe}$ sample.

Four phases, A, B, C, and D, can be clearly distinguished in the temporal development of the diffraction efficiency $\eta(t)$ of Fig. 3. We can give the following interpretation for the observed behavior. In phase A of $\eta(t)$ the primary charge carriers lead to the buildup of the photoinduced space-charge field, which is then compensated for in phase B by some secondary charge carriers. At the end of phase B two canceling electric-field grating components are generated. At the beginning of phase C the recording beams are switched off, and the grating formed by the primary charge carriers disappears by diffusion. Thus the second grating is revealed and starts to decay exponentially with a different time constant (phase D).

The presence of the two compensating gratings at the end of phase B can be demonstrated in two ways. One possibility is that at that point the crystal could be shifted by a fraction of the fringe spacing. In this way the old primary grating would be erased and a new one, having a different phase, would be generated. If the shift of the crystal were half of the fringe spacing, the new primary space-charge grating and the old secondary grating would add, giving a diffraction efficiency that would be four times larger. The second possibility is simultaneous Bragg-diffraction and beam-coupling measurements. Such measurements are shown in Figure 4. The value of γ_0 during the dark decay is measured by periodically turning on the recording beams for a short time. At the first and second peak of η we have $\gamma_0 < 1$ and $\gamma_0 > 1$, respectively, clearly showing that the primary and secondary gratings are mutually phase shifted by an angle π .

In Fig. 3 both recording beams were switched off at the end of phase B. If only one of the writing beams is interrupted, a nearly identical dynamics is observed. From this it follows directly that the secondary grating cannot be erased optically. A completely different dynamics would otherwise be expected in phases C and D. Figure 5 illustrates an attempt to erase the secondary grating by

homogeneous illumination at 514 nm. The decay velocity of the secondary grating under the homogeneous illumination is even slightly slower than in the dark. The first transient observed immediately after switching on the erasure beam is most likely due to a partial compensation for the secondary grating by the new photoexcited primary charge carriers. This compensation is never complete even for erasure intensities greatly exceeding 1 W/cm^2 . If the homogeneous illumination is again switched off, η recovers its old value.

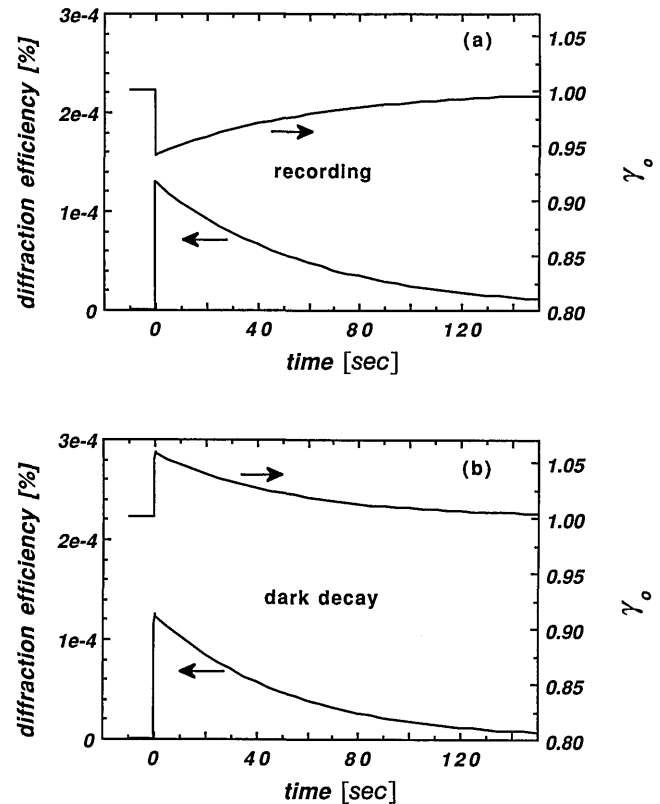


Fig. 4. Simultaneous measurement of diffraction efficiency η (left-hand scales) and effective gain γ_0 (right-hand scales) during (a) recording and (b) subsequent decay in the dark in pure KNbO_3 ($T = 94^\circ\text{C}$).

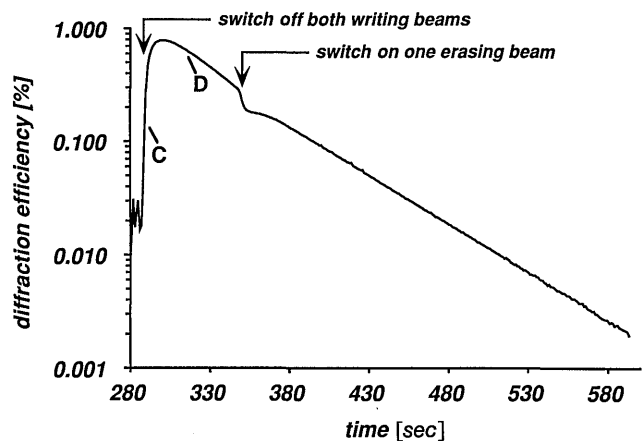


Fig. 5. Attempt to erase a secondary grating during phase D in the $\text{KNbO}_3:\text{LiNaFe}$ sample. Temperature = 102°C . Between $t = 290$ sec and $t = 345$ sec only the weak He-Ne probing beam illuminates the crystal. At $t = 345$ sec an erasing beam ($\lambda = 514.5 \text{ nm}$) with intensity $I = 0.25 \text{ W/cm}^2$ is switched on.

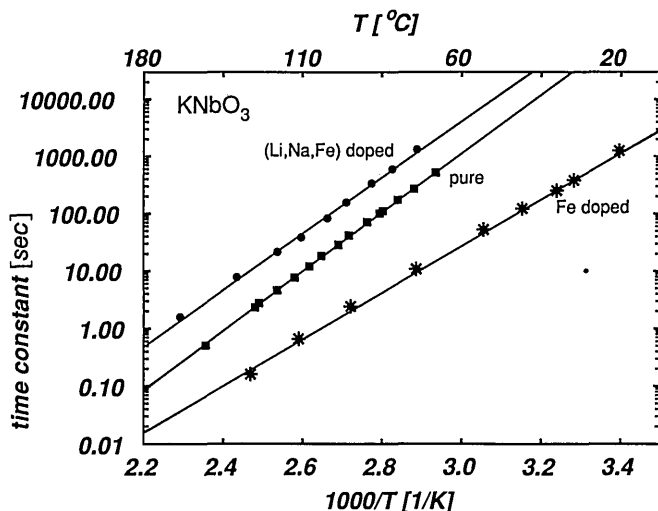


Fig. 6. Time constant τ [Eq. (3)] as a function of the inverse temperature. ●, $\text{KNbO}_3\text{:LiNaFe}$; ■, $\text{KNbO}_3\text{:pure}$; *, $\text{KNbO}_3\text{:Fe}$. The activation energies ΔE are obtained from the linear fits, following Eq. (8). $\Delta E = 0.98$ eV for $\text{KNbO}_3\text{:LiNaFe}$, $\Delta E = 1.04$ eV for $\text{KNbO}_3\text{:pure}$, and $\Delta E = 0.81$ eV for $\text{KNbO}_3\text{:Fe}$.

As can be clearly seen in Fig. 5, the decay of the secondary grating is always a simple exponential, in the dark as well as under homogeneous illumination. The same holds for the time behavior during compensation in phase B (Fig. 3). We can therefore fit the experimental curves in phase D as

$$\Delta n(t) = \Delta n_0 \exp(-t/\tau), \quad (3)$$

where Δn is the amplitude of the refractive-index change. The measured values of the time constant τ at different temperatures can be seen in Fig. 6 for the three different crystals; the longest decay times are obtained in the $\text{KNbO}_3\text{:LiNaFe}$ sample, the shortest in the $\text{KNbO}_3\text{:Fe}$ sample.

From the measured time constants τ [Eq. (3)], some information can be obtained about the mobility of the secondary charge carrier. Let us assume that in phase D only the secondary charge carriers contribute to the space-charge field. The concentration N of the secondary carriers is then given by

$$N(x) = N_0 + N_1 \cos(Kx), \quad (4)$$

where K is the grating vector, N_0 is the average density of the secondary charge carriers, and N_1 the modulation amplitude. The space-charge field produced by this inhomogeneous distribution is obtained by using the Poisson equation:

$$E_{sc}(x) = \frac{eN_1}{\epsilon\epsilon_0 K} \sin(Kx), \quad (5)$$

where ϵ is the dielectric constant and ϵ_0 is the permittivity of the vacuum. The equation for the current density for self-erasure of the secondary grating contains two terms, one due to drift of the secondary charge carriers by the space-charge field and the second due to diffusion,

$$J = e\mu_s N E_{sc} - \mu_s k_B T (\partial N / \partial x). \quad (6)$$

Here k_B is the Boltzmann constant, T is the absolute tem-

perature, and μ_s is the mobility of the secondary charge carriers. Inserting Eqs. (4)–(6) into the continuity equation, we obtain the relation

$$\frac{\partial N_1}{\partial t} = -\frac{e\mu_s N_0}{\epsilon\epsilon_0} N_1 - \frac{\mu_s k_B T K^2}{e} N_1, \quad (7)$$

where $N_0 \gg N_1$ was assumed. This assumption is reasonable, since the observed diffraction efficiencies require a modulation amplitude $N_1 \approx 6 \times 10^{13} \text{ cm}^{-3}$, and, as will be discussed in Section 4, the total number of moving defects N_0 is expected to be 4 or 5 orders of magnitude larger than N_1 . For $T = 200^\circ\text{C}$, $\Lambda = 2\pi/K = 1.75 \mu\text{m}$, and, inserting $\epsilon = 55$ for KNbO_3 , one obtains $k_B T K^2 / e \approx 8 \times 10^{10} \text{ (V/m}^2\text{)}$ and $eN_0 / \epsilon\epsilon_0 \approx 3.3 \times 10^{-10} \text{ V m} \times N_0 \text{ (m}^{-3}\text{)}$. Therefore for $N_0 \geq 3 \times 10^{14} \text{ cm}^{-3}$ the first term on the right-hand side of Eq. (7) dominates, and the exponential time constant τ of Eq. (3) corresponds to the dielectric relaxation time $\epsilon\epsilon_0 / e\mu_s N_0$. From the experimentally measured time constants we can therefore estimate the product $\mu_s N_0$. For $\text{KNbO}_3\text{:LiNaFe}$ we obtain $\mu_s N_0 \approx 7.6 \times 10^6 \text{ (V cm sec)}^{-1}$ at $T = 150^\circ\text{C}$ and $\mu_s N_0 \approx 17 \text{ (V cm sec)}^{-1}$ at room temperature. The values for $\text{KNbO}_3\text{:Fe}$ are $\mu_s N_0 \approx 4.3 \times 10^8 \text{ (V cm sec)}^{-1}$ at $T = 150^\circ$ and $\mu_s N_0 \approx 2.3 \times 10^4 \text{ (V cm sec)}^{-1}$ at $T = 22^\circ\text{C}$. Assuming a defect concentration $N_0 \approx 10^{18} \text{ cm}^{-3}$, the mobility of the secondary charge in $\text{KNbO}_3\text{:LiNaFe}$ can be estimated to vary between $\mu_s \approx 10^{-11} \text{ cm}^2\text{/(V sec)}$ at $T = 150^\circ\text{C}$ and $\mu_s \approx 10^{-17} \text{ cm}^2\text{/(V sec)}$ at room temperature. For $\text{KNbO}_3\text{:Fe}$ we expect $\mu_s \approx 10^{-9}\text{--}10^{-14} \text{ cm}^2\text{/(V sec)}$ for the same temperature range and a similar concentration N_0 . The values for the pure crystal lie between those of the two doped crystals.

As can be seen in Fig. 6, the time constant τ is strongly temperature dependent and follows an Arrhenius law:

$$\tau(T) = \tau_0 \exp(\Delta E / k_B T). \quad (8)$$

Fitting the experimental data to this equation, we can obtain the activation energy ΔE for the mobility of the secondary charge carriers. The activation energies are $\Delta E = 1.04 \pm 0.02$ eV for the pure sample, $\Delta E = 0.98 \pm 0.05$ eV for $\text{KNbO}_3\text{:LiNaFe}$, and $\Delta E = 0.81 \pm 0.05$ eV for $\text{KNbO}_3\text{:Fe}$. The fitted values for the preexponential term τ_0 in Eq. (4) are $\tau_0 = 0.3$ psec for $\text{KNbO}_3\text{:pure}$, $\tau_0 = 10$ psec for $\text{KNbO}_3\text{:LiNaFe}$, and $\tau_0 = 19$ psec for $\text{KNbO}_3\text{:Fe}$.

For $\text{KNbO}_3\text{:LiNaFe}$ and $\text{KNbO}_3\text{:pure}$, ΔE agrees within the experimental error to a value of 1.0 eV. Similar values were obtained in the past from the slope of the dark-conductivity plot versus inverse temperature at temperatures above 100°C . The reported activation energies are $\Delta E = 1.0$ eV for Fe-doped KNbO_3 (Ref. 22) and $\Delta E = 1.2$ eV in pure reduced KNbO_3 .²⁵ The somewhat smaller value of the activation energy observed in our Fe-doped sample (Fig. 6) cannot be explained at the present stage of the investigations.

Fixing of volume holograms can be achieved by using the strong temperature dependence of τ . The hologram is recorded at a given fixing temperature of typically $\sim 80^\circ\text{C}$. After the compensation is accomplished, the crystal is cooled to room temperature. During the cooling process the recording can be either continued or interrupted. In the second case the cooling process should be fast in order

to avoid the backdiffusion of the secondary charge carriers. At room temperature a simple exponential decay of the fixed grating is observed. The corresponding storage times of 20 days for $\text{KNbO}_3:\text{LiNaFe}$, 1 day for KNbO_3 :pure, and 20 min for $\text{KNbO}_3:\text{Fe}$ agree well with the extrapolation of the fitted straight lines in Fig. 6. Further cooling of the $\text{KNbO}_3:\text{LiNaFe}$ sample to 0°C can lead to optically nonerasable holograms with a storage time of 6 months, corresponding to an improvement by 7 orders of magnitude with respect to a nonfixed grating. Because of the faster diffusion of the secondary charge carriers, holograms in the $\text{KNbO}_3:\text{Fe}$ sample can be fixed even at room temperature without the need for an applied electric field. However, in this case there is the basic disadvantage that the time required for the fixation and the storage time are more or less equal. The diffraction efficiencies obtained for the fixed grating are typically between one tenth and one half of the values measured for the primary grating alone and reach $\sim 0.5\%$ in our 1.5-mm-thick samples.

4. DISCUSSION

The anomalous behavior at elevated temperatures and the fixing characteristics were explained in Section 3 in terms of some thermally activated carriers migrating in the crystal. The origin of the carriers was not determined. The photorefractive characteristics (e.g., the sign of the primary charge carriers) of the three investigated samples are different. Nevertheless, the same anomalous behavior is observed in all samples investigated. Based on this fact, some conclusions can be drawn about the nature of the involved secondary charge carriers. For the following discussion, we make the basic assumption that the origin of the secondary carriers is the same in all the investigated samples. This seems reasonable for two reasons. First, in the three crystals the dynamics is the same; second, apart from the $\text{KNbO}_3:\text{Fe}$ sample, the activation energies are quite close to each other in the $\text{KNbO}_3:\text{LiNaFe}$ and the KNbO_3 :pure samples.

It may be suggested that primary and secondary charge carriers are both of an electronic nature but have a different sign (e.g., electrons and holes). A similar kind of charge transport is believed to be responsible for the room-temperature holographic fixing in BSO and BTO.¹⁷⁻¹⁹ In this case a model with two completely independent sets of active centers like the one proposed by Valley²⁶ should be assumed. Only one of the sets should be photoactive, in order to prevent erasure by photoexcitation. One of the two sets should provide only excitation of electrons into the conduction band and the other only hole excitation in the valence band. Such a model could account for our observations only if the different samples are considered individually. For instance, in $\text{KNbO}_3:\text{Fe}$ or $\text{KNbO}_3:\text{LiNaFe}$ a photoinduced grating formed by holes could be compensated by thermally excited electrons that represent the secondary carriers. If the mobility and the cross section for thermal excitation of the electrons are low, the electron grating will remain stored for a long time. Since the photo cross section for electrons is zero and the two sets are independent, an optical erasure would be prevented.

If the results obtained for the different samples are compared and our basic assumption is taken into account,

the above model fails. In the two doped samples, where the primary charge carriers are represented by holes, the model would require that the compensation charge carriers be electrons. The contrary would be true for the undoped crystal. This is clearly in contrast with the assumption of a common origin of the secondary charge carriers for all samples. A further argument can be given to demonstrate the unsuitability of the above model for the explanation of hologram fixing in KNbO_3 . The primary charge carriers in $\text{KNbO}_3:\text{LiNaFe}$ were changed from holes to electrons after application of an electric field of approximately 100 V/cm at 180°C for 14 h. After this treatment the crystal still showed the same unusual dynamics without any relevant change in the time constants for the compensating grating and the related activation energy defined in Eq. (8). This shows that the secondary carriers also remained the same after the reduction treatment and, since the fixed gratings were still not erasable, the identification of the secondary carriers as electrons or holes can be excluded.

The observed effects can be understood only if besides band motion another kind of charge transport is considered, e.g., the motion of some ions in the bulk of the crystal. This accounts for the impossibility of optical erasure of the grating, since ionic motion cannot be activated directly by photons.

In LiNbO_3 the motion of protons seems to contribute to the fixing mechanism.²⁷ Their thermal activation energy is 1.1 eV and lies quite close to the values that were measured in this work for KNbO_3 . The protons form OH^- groups inside the crystal, and the connected vibrational absorption band in the infrared can be measured. In this way the presence of protons in an amount normally exceeding 10^{18} cm^{-3} was demonstrated in the case of KNbO_3 crystals also.²⁸ It is therefore possible that protons are responsible for the fixing in our samples. However, data about their mobility are not yet available, and a definitive assignment is not possible at the present stage of the investigations.

In a recent paper, Matull and Rupp²⁹ proposed a connection between the thermal fixing of holograms and the thermoelectret properties in the case of LiNbO_3 . Since the two phenomena are quite similar, the assumption of a common microscopical origin seems reasonable and could probably be applied to most of the materials that permit high-temperature thermal fixing. The existence of an electret state in a number of ABO_3 oxides with the perovskite structure was demonstrated recently.³⁰ It was shown that a high concentration of A and O vacancies favor the formation of thermoelectrets. The role played by the diffusion of oxygen vacancies in the formation and discharge of the electrets was also emphasized in a paper by Bondarenko *et al.*³¹ Further arguments suggest a possible relation of hologram fixing to diffusion of oxygen vacancies. The electrocoloration of SrTiO_3 at temperatures above 100°C was attributed to the drift of oxygen vacancies that creates reduced and oxidized regions in the crystal.³² The authors estimated an oxygen vacancy concentration N_V of 10^{18} cm^{-3} and a mobility μ_V of $10^{-8}\text{ cm}^2/\text{V sec}$ at 200°C . The related activation energy varies in SrTiO_3 between ~ 0.7 and ~ 1.0 eV. In other perovskite materials like KNbO_3 and BaTiO_3 similar values may be expected. Indeed, the above values for N_V and μ_V are con-

sistent with our measurements of the dielectric time constants during the decay of the secondary grating within 2 orders of magnitude in all the investigated samples (e.g., $N_0\mu_s \approx 10^8$ (V cm sec) $^{-1}$ in $\text{KNbO}_3\text{:LiNaFe}$ at 200°C). Moreover, the respective activation energies are also consistent with our experiments. If vacancy diffusion is responsible for the fixing in KNbO_3 , the different time constants observed for the three different crystals could be explained by a different vacancy concentration that is due to slightly different growing conditions or by a different mobility that is due to different scattering mechanisms induced by the different dopants. However, the actual data seem to support explanations by means of either a proton or a vacancy mechanism and do not permit a definitive attribution.

In conclusion, the possibility of using KNbO_3 as a long-term storage medium was demonstrated. The largest increase of the storage time (6 orders of magnitude at room temperature) was reached for the $\text{KNbO}_3\text{:LiNaFe}$ crystal. The doping has been shown to influence strongly the thermal fixing characteristics of KNbO_3 . This allows us to expect a further optimization of the storage times in new doped crystals that are being grown now. A purely electronic mechanism can be excluded, and the drift of ions in the bulk of the crystal can explain the observed phenomena. The moving microscopical defects are suggested to be either protons or oxygen vacancies. However, more work is needed in order to identify clearly which one of the two defects plays the significant role.

ACKNOWLEDGMENTS

We thank J. Hulliger and H. Wüest for the crystal growth and J. Hajfler for his expert sample polishing. This work was supported by the Swiss National Science Foundation (NFP 13:Microelectronics and Optoelectronics).

REFERENCES

- P. Günter, "Holography, coherent light amplification and optical phase conjugation with photorefractive materials," *Phys. Rep.* **93**, 199–299 (1982).
- P. Günter and F. Micheron, "Photorefractive effects and photocurrents in $\text{KNbO}_3\text{:Fe}$," *Ferroelectrics* **18**, 27–38 (1978).
- P. Günter, "Electro-optical properties of KNbO_3 ," *Opt. Commun.* **11**, 285–290 (1974).
- C. Medrano, E. Voit, P. Amrhein, and P. Günter, "Optimization of the photorefractive properties of KNbO_3 crystals," *J. Appl. Phys.* **64**, 4668–4673 (1988).
- P. Günter and A. Krumins, "High-sensitivity read-write volume holographic storage in reduced KNbO_3 crystals," *Appl. Phys.* **23**, 199–207 (1980).
- P. Günter, "Coherent light amplification and optical phase conjugation in photoconductive electro-optic materials," *Ferroelectrics* **40**, 43–47 (1982).
- J. J. Amoedi and D. L. Staebler, "Holographic pattern fixing in electro-optic crystals," *Appl. Phys. Lett.* **18**, 540–542 (1971).
- D. L. Staebler, "Ferroelectric crystals," in *Holographic Recording Materials*, H. M. Smith, ed. (Springer-Verlag, Berlin, 1977), pp. 101–132.
- L. Arizmendi, "Thermal fixing of holographic gratings in $\text{Bi}_{12}\text{SiO}_{20}$," *J. Appl. Phys.* **65**, 423–427 (1989).
- F. Micheron and G. Bismuth, "Electrical control of fixation and erasure of holographic patterns in ferroelectric materials," *Appl. Phys. Lett.* **20**, 79–81 (1972).
- J. B. Thaxter and M. Kestigian, "Unique properties of SBN and their use in a layered optical memory," *Appl. Opt.* **13**, 913–924 (1974).
- S. Redfield and L. Hesselink, "Enhanced nondestructive holographic readout in strontium barium niobate," *Opt. Lett.* **13**, 880–882 (1988).
- D. von der Linde, A. M. Glass, and K. F. Rogers, "Multiphoton photorefractive processes for optical storage in LiNbO_3 ," *Appl. Phys. Lett.* **25**, 155–157 (1974).
- D. von der Linde, A. M. Glass, and K. F. Rogers, "High-sensitivity optical recording in KTN by two photon absorption," *Appl. Phys. Lett.* **26**, 22–24 (1975).
- S. W. McCahon, D. Rytz, G. C. Valley, M. B. Klein, and B. A. Wechsler, "Hologram fixing in $\text{Bi}_{12}\text{TiO}_{20}$ using heating and an ac electric field," *Appl. Opt.* **28**, 1967–1969 (1989).
- G. S. Trofimov and S. I. Stepanov, "Electrical development of a hologram in a $\text{Bi}_{12}\text{SiO}_{20}$ crystal," *Sov. Tech. Phys. Lett.* **10**, 282–283 (1984).
- J. P. Herriau and J. P. Huignard, "Hologram fixing process at room temperature in photorefractive $\text{Bi}_{12}\text{SiO}_{20}$ crystals," *Appl. Phys. Lett.* **49**, 1140–1142 (1986).
- A. Delboulbe, C. Fromont, J. P. Herriau, S. Mallick, and J. P. Huignard, "Quasi-nondestructive readout of holographically stored information in photorefractive $\text{Bi}_{12}\text{SiO}_{20}$ crystals," *Appl. Phys. Lett.* **55**, 713–715 (1989).
- M. Miteva and L. Nikolova, "Oscillating behavior of diffracted light on uniform illumination of holograms in photorefractive $\text{Bi}_{12}\text{TiO}_{20}$ crystals," *Opt. Commun.* **67**, 192–194 (1988).
- G. Montemezzani, M. Ingold, H. Looser, and P. Günter, "Multiple photorefractive gratings in Ce-doped LiNbO_3 and KNbO_3 crystals," *Ferroelectrics* **92**, 281–287 (1989).
- Wu Xing, H. Looser, H. Wüest, and H. Arend, "Progress in KNbO_3 crystal growth," *J. Cryst. Growth* **78**, 431–437 (1986).
- E. Voit, "Photorefractive properties and applications of KNbO_3 crystals," Ph.D. dissertation ETH Nr. 8555 (Swiss Federal Institute of Technology, Zürich, 1988).
- E. Krätzig, "Photorefractive effects and photoconductivity in $\text{LiNbO}_3\text{:Fe}$," *Ferroelectrics* **21**, 635–636 (1978).
- R. Orłowski and E. Krätzig, "Holographic method for the determination of photo-induced electron and hole transport in electro-optic crystals," *Solid State Commun.* **27**, 1351–1354 (1978).
- A. E. Krumins and P. Günter, "Photovoltaic effect and photoconductivity in reduced potassium niobate crystals," *Phys. Status Solidi A* **55**, K185–K189 (1979).
- G. C. Valley, "Simultaneous electron/hole transport in photorefractive materials," *J. Appl. Phys.* **59**, 3363–3366 (1986).
- H. Vormann, G. Weber, S. Kapphan, and E. Krätzig, "Hydrogen as origin of thermal fixing in $\text{LiNbO}_3\text{:Fe}$," *Solid State Commun.* **40**, 543–545 (1981).
- A. Förster, H. Hesse, S. Kapphan, and M. Wöhlecke, "OH stretching vibrations in monodomain KNbO_3 ," *Solid State Commun.* **57**, 373–375 (1986).
- R. Matull and R. A. Rupp, "Microphotometric investigation of fixed holograms," *J. Phys. D* **21**, 1556–1565 (1988).
- E. M. Panchenko, O. I. Prokopalo, A. E. Panich, V. A. Zagoruiko, and Yu. A. Trusov, "Electret state in oxides of the perovskite family," *J. Phys. D* **22**, 1372–1374 (1989).
- E. I. Bondarenko, V. A. Zagorulko, Yu. S. Kuz'minov, A. N. Pavlov, E. M. Panchenko, and O. I. Prokopalo, "Model of the electret state in oxygen-octahedral materials," *Sov. Phys. Solid State* **27**, 629–630 (1985).
- J. Blanc and D. L. Staebler, "Electrocoloration in SrTiO_3 : vacancy drift and oxidation-reduction of transition metals," *Phys. Rev. B* **4**, 3548–3557 (1971).